Structure−Function Relationships of the Intact aIF2α Subunit from the Archaeon *Pyrococcus abyssi*[†,‡]

Laure Yatime, Emmanuelle Schmitt,* Sylvain Blanquet, and Yves Mechulam

Laboratoire de Biochimie, Unité Mixte de Recherche 7654, CNRS-Ecole Polytechnique, F-91128 Palaiseau Cedex, France

Received February 28, 2005; Revised Manuscript Received April 28, 2005

ABSTRACT: Eukaryotic and archaeal initiation factor 2 (e- and aIF2, respectively) are heterotrimeric proteins (α*βγ*) supplying the small subunit of the ribosome with methionylated initiator tRNA. The *γ* subunit forms the core of the heterotrimer. It resembles elongation factor EF1-A and ensures interaction with Met-tRNA$_i^{Met}$. In the presence of the α subunit, which is composed of three domains, the *γ* subunit expresses full tRNA binding capacity. This study reports the crystallographic structure of the intact aIF2α subunit from the archaeon *Pyrococcus abyssi* and that of a derived C-terminal fragment containing domains 2 and 3. The obtained structures are compared with those of N-terminal domains 1 and 2 of yeast and human eIF2α and with the recently determined NMR structure of human eIF2α. We show that the three-domain organization in the α subunit is conserved in archaea and eukarya. Domains 1 and 2 form a rigid body linked to a mobile third domain. Sequence comparisons establish that the most conserved regions in the aIF2α polypeptide lie at opposite sides of the protein, within domain 1 and domain 3, respectively. These two domains are known to exhibit RNA binding capacities. We propose that domain 3, which is known to glue the α subunit onto the *γ* subunit, participates in Met-tRNA$_i^{Met}$ binding while domain 1 recognizes either rRNA or mRNA on the ribosome. Thereby, the observed structural mobility within the e- and aIF2α molecules would be an integral part of the biological function of this subunit in the heterotrimeric e- and aIF2α*βγ* factors.

In eukaryotes and archaea, the e- and aIF2[1] factors, respectively, play a crucial role in the process of initiation of translation. In the presence of GTP, this factor delivers the methionylated initiator tRNA to the small subunit of the ribosome. After correct pairing between the AUG initiation codon on mRNA and the CAU anticodon of the methionylated initiator tRNA, GTP is hydrolyzed and e- or aIF2 is released from the ribosome. In eukaryotes, eIF2·GDP is regenerated through the action of a heteropentameric guanine nucleotide exchange factor eIF2B (*1*). In archaea, which do not have any equivalent of eIF2B, the exchange between GDP and GTP is thought to be spontaneous (*2*).

e/aIF2 results from the association of three subunits, α, *β*, and *γ*. The *γ* subunit forms the core of the heterotrimer. It interacts with both the α and *β* proteins. In the trimer, the α and *β* subunits do not interact with one another (*3*, *4*). The structure of aIF2*γ* from *Pyrococcus abyssi* (45 kDa) (*3*) and that of aIF2*γ* from *Methanococcus jannaschii* (*5*) were previously determined. aIF2*γ* is made of three domains. Domain 1 is built around a Rossmann fold and contains the nucleotide binding site, while domains 2 and 3 are *β* barrels. The structure of aIF2*γ* is closely similar to that of elongation factor Tu in its active conformation, that is, bound to GTP and aminoacylated tRNA (*3*, *6*). On the basis of this homology, a model of docking of Met-tRNA$_i^{Met}$ onto aIF2*γ* could be proposed. Additionally, comparison of EF-Tu with aIF2*γ* highlighted specific regions of the initiation factor. These regions can be assumed to participate in binding to the α or *β* subunit and/or binding of Met-tRNA$_i^{Met}$ (*3*). By using site-directed mutagenesis and enzymatic assays, it was further shown that one of the regions of domain 2 of aIF2*γ*, which is specific to the initiation factor, is indeed involved in the binding of aIF2α (*5*, *7*).

e/aIF2α is composed of three domains. The crystal structures of N-terminal segments of human and yeast eIF2α were previously determined (*8*, *9*). These segments comprise two of the three eIF2α domains, an N-terminal *β* barrel followed by a helical domain. On another hand, the C-terminal domain (domain 3 or αD3) of aIF2α was shown to be responsible for the anchoring of the α subunit to the *γ* one (*7*). Furthermore, using assays of protection of Met-tRNA$_i^{Met}$ against deacylation, a reinforcement of the affinity of aIF2*γ* for Met-tRNA$_i^{Met}$ was observed in the presence of the α subunit. Actually, domain 3 of the α subunit is sufficient to give an αD3*γ* dimer its full tRNA binding capacity, as compared to the intact aIF2 trimer (*7*).

The aim of this study was to determine the three-dimensional (3D) structure of the α subunit of an archaeal aIF2. The X-ray structures of both the full-length aIF2α from *P. abyssi* (32 kDa) and of a C-terminal fragment containing domains 2 and 3 (αD2−3) were determined at 3.37 and 2.26 Å resolution, respectively. The structure of αD3 is in agreement with that of the corresponding domain in the recently determined NMR structure of human eIF2 (*10*). We

[†] L.Y. was a recipient of a Monge doctoral fellowship from Ecole Polytechnique.

[‡] The coordinates have been deposited in the Protein Data Bank as entries 1YZ6 and 1YZ7.

* To whom correspondence should be addressed. E-mail: emma@botrytis.polytechnique.fr. Phone: +33 1 69334181. Fax: +33 1 69333013.

[1] Abbreviations: eIF2, eukaryotic initiation factor 2; aIF2, archaeal initiation factor 2.

10.1021/bi050373i CCC: $30.25
Published on Web 05/27/2005

show that this αD3 domain presents a versatile βαββαβ fold that is found in various types of proteins (*11*−*13*). Moreover, comparison of the structure of *P. abyssi* aIF2α with those of the N-terminal fragment (αD1−2) of yeast and human eIF2α (*8*−*10*) shows that domains 1 and 2 have constant relative orientations. In contrast, comparison of the structure of αD2−3 with that of full-length aIF2α shows that the two rigid bodies, αD1−2 and αD3, are connected by a flexible linker. Relative mobility between these two parts of the protein has already been suggested on the basis of the NMR structure of human eIF2α (*10*). Together, these structural data establish that the organization of e/aIF2α is conserved in the archaeal and eukaryal translation systems.

Finally, we observe that the most conserved regions of aIF2α lie on opposite sides of the protein, within domain 1 and domain 3. These two domains are known to exhibit RNA binding capacities (*7*). We suggest that domain 3 interacts with Met-tRNA$_i^{Met}$, while domain 1 might recognize either rRNA or mRNA. In this context, the observed structural mobility within the α fold would underlie the biological function of this subunit in the heterotrimeric factor.

EXPERIMENTAL PROCEDURES

Expression and Purification of the aIF2α Variants

Expression and Purification of Native aIF2α. Plasmid pET3aαpa encoding the α subunit of *P. abyssi* aIF2 (*3*) was introduced into *Escherichia coli* BL21 cells together with the tRNA$_4^{Arg}$-overexpressing pSBETa plasmid (*14*). *E. coli* cultures were grown in 2×TY medium containing 50 μg/mL ampilicillin and 25 μg/mL kanamycin. Expression of the α subunit was induced by adding IPTG to a concentration of 1 mM when the OD_{650} of the culture reached 1.6. The culture was then continued for 12 h at room temperature. Purification of aIF2α was as described in ref *3*. Briefly, the heated crude extract was loaded onto a Q-Hiload (16 mm × 12 cm; Amersham) column equilibrated in buffer A [500 mM NaCl, 10 mM MOPS (pH 6.7), and 10 mM 2-mercaptoethanol]. The flow through was recovered and dialyzed against a buffer made of 300 mM NaCl, 10 mM MOPS (pH 6.7), and 10 mM 2-mercaptoethanol. The dialyzed sample was then loaded onto a MonoS column (5 mm × 5 cm; Amersham) equilibrated in the same buffer and eluted with a gradient from 0.3 to 0.8 M NaCl in 15 mL. The eluted peak containing the protein was finally loaded onto a Superdex75 column (16 mm × 60 cm; Amersham) equilibrated in buffer A. Recovered protein was concentrated using a Centricon 30 concentrator and used for crystallization trials.

Expression of αD2−3 and Purification of Selenomethionylated and Native αD2−3 Proteins. The DNA encoding αD2−3 was obtained by PCR amplification with the introduction of a start codon at position 88 of the open reading frame for the α subunit. The obtained DNA fragment was recloned in pET3a-lpa (*7*). The αD2−3 protein was expressed and purified using the same protocol that was used for aIF2α. However, because of the acidic isolectric point of the αD2−3 protein, the MonoS step of aIF2α purification was replaced with a MonoQ one, as described in ref *7*.

αD2−3 protein does not contain any methionine. Therefore, to incorporate selenomethionine, it was necessary to modify the gene encoding αD2−3 by site-directed mutagenesis. Two methionine codons were introduced: one at position 106 (domain 2) and the other at position 184 (domain 3). These two positions were chosen after sequence comparisons of aIF2α proteins and identification of positions where methionine residues are encountered. Site-directed mutageneses were achieved in one step using two mutagenic primers and PfuTurbo DNA polymerase (Stratagene). The first primer (5′GCTCAGAAGGCAGAGAATATGCTCAAGCTCGCGGCCGAA) introduces a Met codon at position 106 on one strand, and the second one (5′ATTTGGCTTTGGAACCGTCATCTCGAACTCCGCATCTAT) introduces a Met codon at position 184 on the complementary strand. After thermal cycling, methylated wild-type DNA was restricted in the presence of *Dpn*I before transformation of XL1-Blue cells. The sequence of the whole mutated αD2−3 gene was then verified. The obtained mutant plasmid pET3aαD2−3 was transformed with pSBETa into the methionine auxotroph B834-De3 strain (Novagen). Transformed cells were grown overnight in 60 mL of LB medium. This starter culture was harvested, and washed cells were then resuspended in 30 mL of M9 minimal medium. A portion (2.5 mL) of this cell suspension were used to inoculate 1 L of M9 minimal medium containing 15 mg of selenomethionine (Sigma). The selenomethionylated protein was purified as the native one.

Crystallization

Initial screening for crystallization conditions with aIF2α was performed with the hanging drop technique, by using protein at 15 mg/mL in a buffer made of 500 mM NaCl, 10 mM MOPS (pH 6.7), 10 mM 2-mercaptoethanol, and a homemade ammonium sulfate screen. Crystals were obtained within 2 days using 0.6 M ammonium sulfate and 0.1 M NaAc (pH 5.0). For data collection, these crystals were soaked in 40% ethylene glycol, 0.5 M ammonium sulfate, and 0.83 M NaAc (pH 5.0) as a cryoprotectant and flash-cooled in liquid ethane. The crystals belonged to space group $P3_121$ and diffracted to 3.37 Å resolution (Table 1).

Crystals of aIF2αD2−3 were obtained with the hanging drop technique using a TECAN genesis rsp100 robot and commercial screens from Hampton Research. Native crystals were grown at 24 °C in 2.0 M ammonium sulfate and 5% 2-propanol, using protein at 7 or 14 mg/mL in a buffer containing 200 mM NaCl, 10 mM MOPS (pH 6.7), and 10 mM 2-mercaptoethanol. Crystals of the selenomethionylated protein were obtained and handled using the same conditions. Before data collection, crystals were soaked in a solution containing 2.0 M ammonium sulfate and 25% glycerol and flash-cooled either directly within a nitrogen gas stream or in liquid ethane. Native crystals belonged to space group $P2_12_12$ and diffracted to 2.26 Å resolution.

Structure Determination and Refinement

Data corresponding to α and αD2−3 crystals were collected at 100 K by using synchrotron sources at the ESRF [Grenoble, France; ID14eh1 and ID23 beamlines (Table 1)]. Diffraction images were analyzed using MOSFLM (*15*). Data were processed further with programs of the CCP4 package (*16*).

αD2−3. One two-wavelength data set with a Se-Met crystal was collected at the ID23eh1 beamline (Table 1,

Table 1: Native and Selenomethionylated Derivative Data Used in This Study

	α2−3 native	α2−3 Semet		α
wavelength (Å)	0.9340	0.979	0.9756	0.934
X-ray source	id14eh1	id23		id14eh1
space group	$P2_12_12$	$P2_12_12$		$P3_121$
cell parameters *a*, *b*, *c* (Å)	61.5, 79.8, 47.9	63.5, 80.8, 47		104.3, 104.3, 129.4
no. of unique reflections	11532	5906	5896	11911
resolution (Å)	2.26	2.8	2.8	3.37
completeness (%)	99.7	94	93.6	100
anomalous data (%)		85.8	85.6	
redundancy	3.4	3.7	3.6	5.4
R_{sym} (*I*) (%)[a]	4.7 (30.7)	6.0 (36.3)	5.9 (40)	5.8 (33.5)
mean figure of merit		0.35 (20−2.8)		
R/R_{free}[b] (%)	23.6/28.5			24.9/29.0
rmsd for bonds (Å)	0.0077			0.0094
rmsd for angles (deg)	1.32			1.49
B value (Å^2) for protein	45.1			105
B value (Å^2) for water	51.6 (65 waters)			

[a] Values in parentheses are R_{sym} (*I*) in the highest shell of resolution. [b] R_{free} is calculated with 6% of the reflections.

ESRF). The derivative data sets were then input into SOLVE (*17*), and the two expected selenium sites were found and refined. These sites were further used to phase the reflections and to compute initial maps with an average figure of merit of 0.35 for data to 2.8 Å resolution. Maps were improved by solvent flattening and maximum-likelihood density modification using RESOLVE (*18*). The quality of the maps was sufficient to position the model corresponding to aIF2α domain 2 from human (*8*) and to visualize the electron density corresponding to domain 3. The construction was achieved using O (*19*). The structure was refined by cycles of manual model building and energy minimization using CNS (*20*). The final working and R_{free} values for αD2−3 were 23.5 and 28.2%, respectively.

aIF2α. The structure of aIF2α was determined by molecular replacement using PHASER (*21*). Domain 3 was searched first by using domain 3 from the above αD2−3 structure as a model (*Z* score = 17.2). In a second step, domain 2 was searched by using domain 2 from the αD2−3 structure as a model (*Z* score = 14.9). Finally, the position of domain 1 from yeast (*9*) was searched (*Z* score = 10.9). Three unique solutions were found and used to calculate the initial map. The structure was refined by cycles of manual model building and energy minimization with CNS using data between 12 and 3.37 Å resolution (2σ cutoff) (*20*). *B* values were refined for groups of atoms. The obtained average *B* value (105 Å^2) is in accord with the *B* value (90 Å) determined from the Wilson plot. The high *B* value reflects the low diffraction power of the crystals and the high solvent content (76%). The final working *R*-factor and R_{free} for aIF2α were 24.9 and 29.0%, respectively.

Sequence Conservation Analysis

Sixty-six sequences of e/aIF2α were identified using the BLAST resource of the PubMed database (www.ncbi.nlm-.nih.gov/blast). The *P. abyssi* aIF2α sequence was used as a query. This set contains 43 eukaryal and 23 archaeal proteins. The sequences were aligned using Clustal X (*22*). Conservations at each position were then analyzed using Plotsimilarity of the GCG package available at the Infobiogen Web site (www.infobiogen.fr), using a window of five residues. The Blosum 62 similarity matrix was used in this step. In Figure 4, the ribbon has been colored to reflect the result of this sequence analysis.

RESULTS AND DISCUSSION

Overall Structure of aIF2αD2−3

The αD2−3 fragment of aIF2α that we produced contains residues 91−275. Crystals of the native fragment and of the mutant selenomethionylated fragment (see Experimental Procedures) were obtained by using ammonium sulfate as the precipitating agent. The 3D structure was determined by using multiple-anomalous scattering data (MAD, Table 1). After phasing, the quality of the electron density map was sufficient to position the model corresponding to domain 2 of human eIF2α [PDB entry 1KL9 (*8*)] and to clearly show the part of the electron density corresponding to the C-terminal domain of aIF2α (domain 3). After multiple rounds of manual rebuilding and minimization steps, the 3D structure was refined at 2.26 Å resolution with an *R*-factor of 23.5% (R_{free} = 28.2%).

The determined structure consists of two domains linked by a well-defined extended peptide. Interestingly, no interaction is visible between domains 2 and 3 (Figure 1). Domain 2 (residues 91−171) corresponds to five antiparallel α helices closely packed together. This domain can be fully superimposed on the corresponding domains in the human or yeast (PDB entry 1KL9 or 1Q46, respectively) N-terminal eIF2α structure (*8*, *9*) (Figure 1). Identical rms deviations of 1.6 Å for 78 compared C-α atoms were measured when archaeal domain 2 was superimposed onto either the human one or the yeast one.

In domain 3 of the αD2−3 fragment of aIF2α, residues 172−266 fold with a $\beta\alpha\beta\beta\alpha\beta$ topology. The C-terminal peptide, which is composed of residues 267−275, has no defined structure in the electron density, therefore suggesting its mobility in the crystal. The two α helices are located on the same side of a β sheet formed by strands β7, β8, β6, and β9. As a result, the 3D structure of the C domain presents an internal pseudo-2-fold axis of symmetry. The two orientations of domain 3 resulting from this symmetry axis can be superimposed with an rms value of 2.0 Å for 81 compared C-α atoms. Recently, the structure of human eIF2α was determined by NMR. In this structure, the eIF2α C-terminal domain can be superimposed on that of domain 3 of *P. abyssi* aIF2α, with an rms deviation of 1.5 Å for 83 compared C-α atoms. Note that like eukaryotic α subunits, human eIF2α possesses a C-terminal acidic extension absent in the archaeal protein (Figure 2).

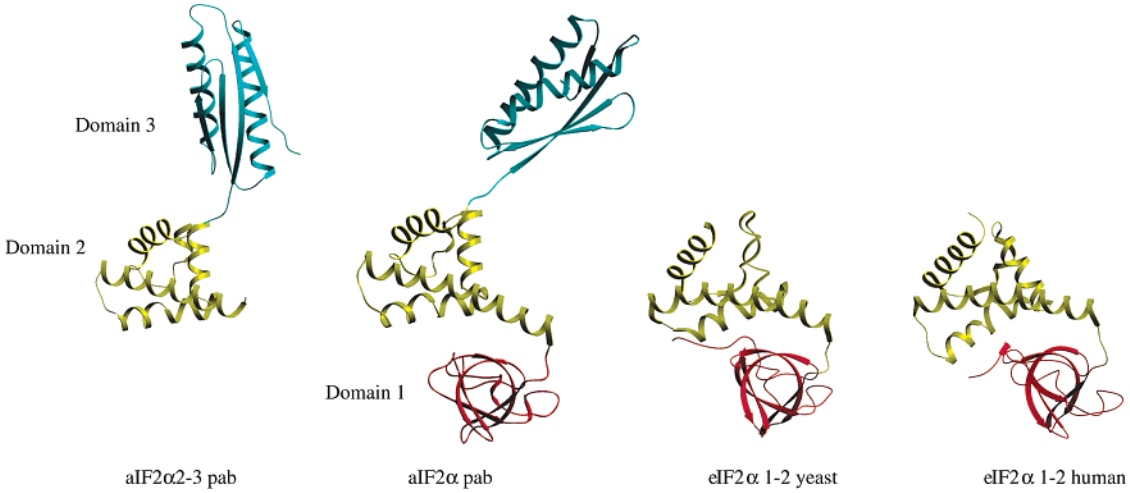

FIGURE 1: Domain arrangement in e/aIF2α structures. The structures of domains 2 and 3 of aIF2α from *P. abyssi*, of full-length aIF2α from *P. abyssi*, of domains 1 and 2 of eIF2α from *Saccharomyces cerevisiae* (*9*), and of domains 1 and 2 of human eIF2α (*8, 10*) are represented as ribbons. The three structural domains are colored as follows: domain 1 (residues 1−84, aIF2αPab numbering) in red, domain 2 (residues 85−171) in yellow, and domain 3 (residues 172−266) in cyan. The domain 2 segments of the four structures were superimposed. Each protein was then drawn according to the resulting orientation. The figure shows that domains 1 and 2 have constant relative orientations, while the orientation of domain 3 varies. Domain 1 is a β barrel homologous to eIF1-A. Domain 2 is α helical and shares similarity with a DNA binding domain found in endonuclease III (*33*). Domain 3 is built around the versatile $\beta\alpha\beta\beta\alpha\beta$ fold. This figure was drawn with Setor (*34*).

The Structure of the Entire aIF2α from P. abyssi Reveals Mobility of Domain 3 with Respect to Domains 1 and 2

Crystals of the intact aIF2α subunit were obtained by using ammonium sulfate as a precipitating agent. A complete data set was collected at 3.37 Å resolution. The structure of the intact subunit was determined by molecular replacement using PHASER (*21*). Three independent modules were used as models: domain 1 (residues 2−91) from yeast and domains 2 (residues 91−173) and 3 (residues 173−266) from *P. abyssi* (this study). The position of domain 3 was searched first followed by that of domain 2 and finally that of domain 1. A well-defined solution was obtained for the position of each domain. Notably, no solution is reached if domain 1 or domain 2 is searched first. Therefore, prior determination of the 3D structure of the archaeal domain 3 was essential for phasing the data corresponding to the aIF2α crystals. After cycles of manual rebuilding and minimization, the model corresponding to the entire aIF2α subunit was refined at 3.37 Å resolution with an *R*-factor of 24.9% (R_{free} = 29.0%).

Despite a relatively modest resolution, the three structural modules and the linker peptides are well-defined in the electron density. The structure of domain 1 linked to domain 2 has been superimposed on the corresponding domains in yeast eIF2α (rms = 1.7 Å for 152 compared atoms) or in the human crystallographic structure of eIF2α (rms = 1.8 Å for 143 compared atoms). Therefore, the relative positions of domain 1 and domain 2 are conserved among eukarya and archaea (Figure 1). In eucaryotes, domain 1 carries a phosphorylatable serine (S51 according to yeast numbering). This serine is located in the loop connecting β3 to β4. This loop is partly disordered in human eIF2α (*8*) but is well-defined in the structure of yeast eIF2α (*9*). Phosphorylation of this serine appears to control the rate of the nucleotide exchange process involving eIF2B (*1*). In archaea, there is no homologue of the catalytic subunit of eIF2B, and the serine corresponding to S51 is not conserved (Figure 2). However, it is notable that the loop connecting β3 to β4 in *P. abyssi* aIF2α adopts a conformation identical to that in yeast eIF2α.

In the 3D structure of yeast and human eIF2α, the groove between domains 1 and 2 is filled by an N-terminal extension containing two residues (F7 and Y8 in yeast) highly conserved in all documented eukaryotic α subunits (Figures 2 and 3) (*8*−*10*). These two aromatic side chains ensure van der Waals contacts bridging domain 1 with domain 2. Moreover, Y8 interacts with E37 (strictly conserved in all eukaryotic sequences) and S104 (conserved in 34 sequences of 42), therefore reinforcing the stability of the interface. In animals, eIF2α contains two conserved cysteines (C69 and C97 in humans) that form a disulfide bridge linking domains 1 and 2 (Figure 3) (*8*). In other eukaryotes, only the second cysteine is found. In the yeast eIF2α structure, this cysteine stacks on a valine substituting for the first cysteine of animals (*9*). In the structure of archaeal aIF2α, the above N-terminal extension is absent and the groove between domains 1 and 2 is deeper (Figure 3). The interface is, however, stabilized by a salt bridge between K93 of α4 and E33 located in the loop linking β3 to β4 (Figure 3). These two residues are highly conserved in archaea. The only exception is that of *Halobacterium salinarium* in which correlated replacements are found at these positions with Q instead of E33 and T instead of K93 (Figure 2). The amino group of K93 also interacts with the main chain carbonyl of F14. Therefore, in archaeal and eucaryal aIF2α, a similar orientation of domain 1 with respect to domain 2 is ensured, although the interactions are markedly different. Notably, although the interface groove in the archaeal subunit is deeper than in the eucaryal ones, its acidic character is conserved (Figure 3 and ref *8*). Domain 2 of the intact aIF2α subunit has been superimposed on domain 2 in the αD2−3 fragment. The orientation of domain 3 with respect to domain 2 differs markedly in the two compared structures. Figure 1 shows a rotation of domain 3 of nearly 110°. There is no contact between domains 2 and 3 in aIF2α or in its αD2−3 fragment.

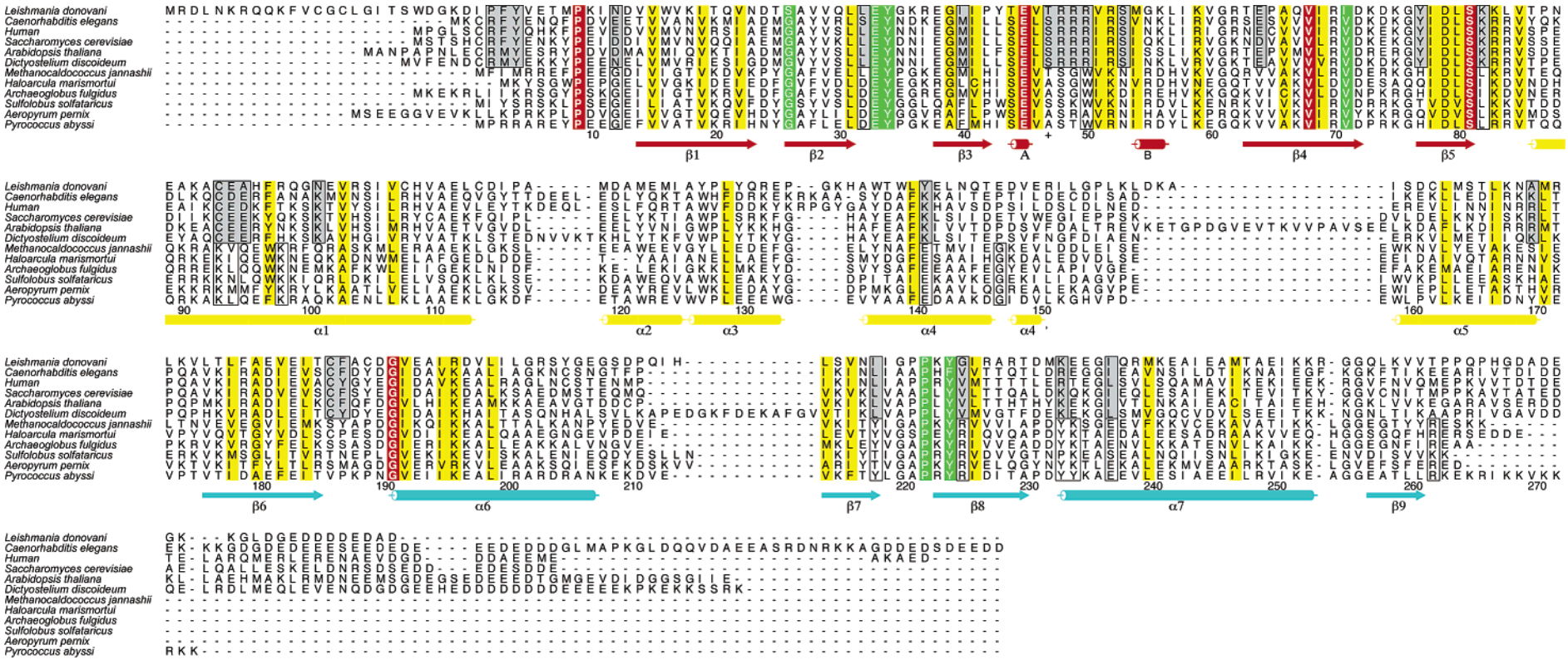

FIGURE 2: Multiple-sequence alignments of eukaryotic and archaeal aIF2α. A total of 66 sequences of eIF2α (43 from eukaryotes and 23 from archaea) were aligned using Clustal X (*22*). For the sake of clarity, only 12 representative sequences are shown (six from eukaryotes and six from archaea). However, conserved residues were identified by considering the whole set of 66 sequences. Strictly conserved residues are printed in white letters and boxed in red. Highly conserved residues (with no more than four exceptions in the 66 sequences) are printed in white letters and boxed in green. Positions with conservative replacements (residue of the same family with no more than two exceptions in the 66 sequences) are highlighted in yellow. Conservation families are as follows: hydrophobic (A, V, L, I, M, F, and C), aromatic (W, Y, and F), basic (R and K), acidic (D and E), polar (T, S, N, Q, and H), and small (G and A). Positions characteristic of eukaryal sequences are highlighted in gray, while positions characteristic of archaeal sequences are boxed. The numbering and the secondary structure elements schematized at the bottom correspond to those of *P. abyssi* aIF2α. The position of the serine target of a specific phosphorylation in eukaryotic eIF2α (S51 in human eIF2α) is indicated by a plus sign below the sequences. This figure was drawn with Alscript (*35*).

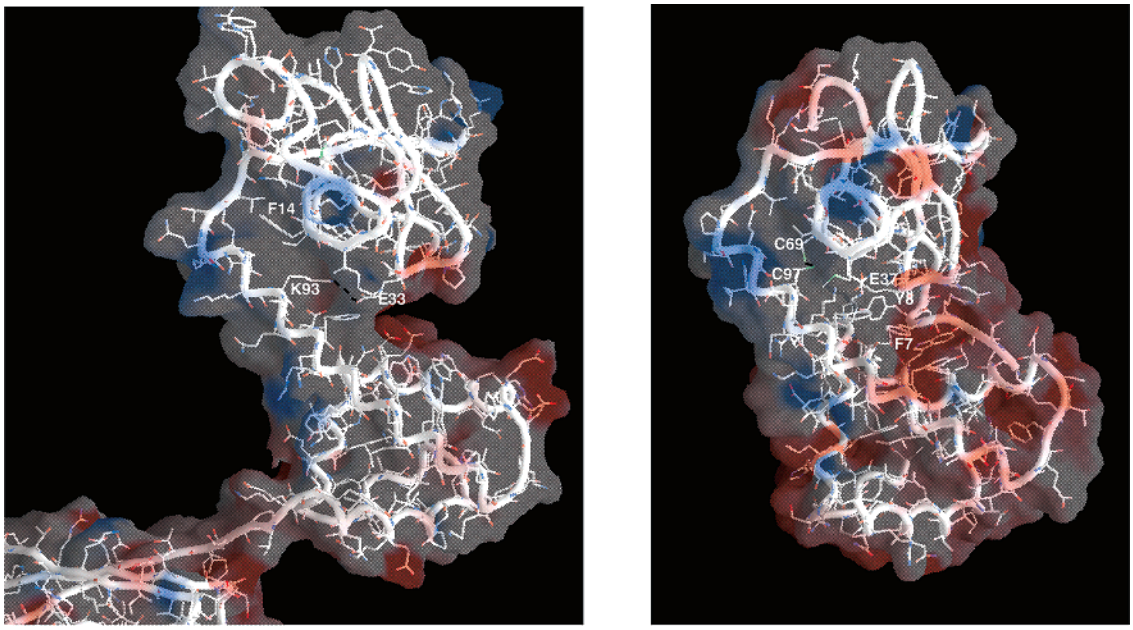

FIGURE 3: Molecular surfaces of *P. abyssi* aIF2α (left) and of an N-terminal fragment of human eIF2α (right) (*8*). This figure shows the electrostatic potentials calculated with Delphi (*36*) and rendered with Grasp (*37*). Negatively charged regions are colored red and positively charged ones blue. The backbones of the two proteins are underlined by a worm, and bonds are drawn as sticks. Residues involved in the interface between domains 1 and 2 are labeled.

These observations are in agreement with the absence of long-range NOEs between domains 1 and 2 and domain 3 of human eIF2α (*10*). In the archaeal protein, movement between domains 2 and 3 arises from a proline (P174) and creates a large variation in the $N-C\alpha_{173}-C-N_{174}$ dihedral angle. This proline is frequently found at position 173 or 174 in the e/aIF2α sequences. Indeed, 56 sequences of 66 compared sequences include this proline (Figure 2). Therefore, mobility between domain 3 on one hand and domains 1 and 2 on the other hand appears to be an important feature of e/aIF2α factors, whatever their origin.

e/aIF2α Displays Two RNA Binding Domains Linked by a Flexible Peptide

Structural Homologies. Domain 1 of aIF2α presents an OB-fold structure made of a five-stranded antiparallel *β* barrel capped by an α helix. This organization is similar to that of domain 1 of the human and yeast proteins. Interestingly, the topology of this OB fold is also encountered in the translation initiation factor e/aIF1-A and in its bacterial homologue IF1. Many RNA binding proteins, such as ribosomal protein S1, PNPases, or aminoacyl-tRNA synthetases, also exhibit such a fold. In all cases, the RNA binding site is formed by the concave side of the barrel (Figure 4). In domain 1 of eIF2α, the long loop between the *β*3 and *β*4 strands harbors a phosphorylatable serine residue (S51 in yeast) that interferes with the recycling of eIF2·GDP to eIF2·GTP (*23*). Since this loop overhangs the OB-folded motif in the α subunit, a possible relationship between the RNA binding properties at the N end of eIF2α factors and regulation of the GDP−GTP exchange in eIF2*γ* may be considered.

A search using the DALI database (www.ebi.ac.uk/dali) reveals that more than 700 proteins share significant homologies with αD3, the C end of the α subunit (*Z* score > 2.0). This structural module, which has a *βαββαβ* topology, is

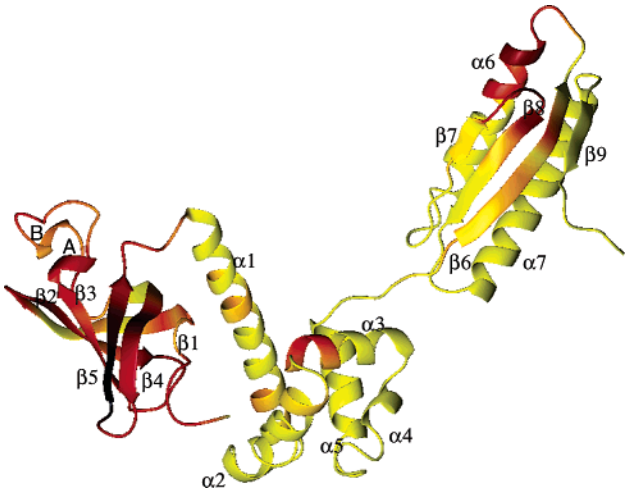

FIGURE 4: Positions of conserved residues in the aIF2α structure. Sequence conservations were analyzed as described in Experimental Procedures (see Figure 2). Residues below the mean level of conservation are colored yellow. Residues between the mean and the maximum are colored on a linear scale from yellow to blue such that red is halfway between the mean and the maximum. This figure was drawn using Molmol (*38*).

therefore very widespread in many proteins, some of which are involved in the translational process, while others have unrelated functions [for example, the RNP domain of U1AsnRNP, PDB entry 1FHT (*24*), or the ATX1 metallo chaperone protein, PDB entry 1CC8 (*25*)]. The αD3-like modules can form a part of a protein, but they can also exist as isolated domains. Because of its broad representation within proteins involved in translation, this module has been proposed to be a fundamental RNA binding motif having emerged early from the RNA world (*12*, *26*). For instance, this domain is found in two tRNA binding proteins: phenylalanyl-tRNA synthetase (*27*; PDB entry 1pys; $Z = 8.5$, rms = 2.3 for 82 atoms) and tRNA nucleotidyl transferase from *Archeoglobus fulgidus* (*28*; PDB entry 1sz1; $Z = 6.0$,

rms = 3.1 for 83 atoms). It is worth noting that among the proteins giving the highest homology scores with αD3, we find domain 3 of the translocase eEF2 (*29*; PDB entry 1n0v; $Z = 7.2$, rms = 1.9 Å for 63 atoms), the ribosomal protein S6 (*13*; PDB entry 1ris; $Z = 6.4$, rms = 2.1 Å for 69 atoms), and the guanine exchange factor eEF1B-β (*11*; PDB entry 1b64; $Z = 6.5$, rms = 2.1 Å for 72 atoms). Homology with guanine exchange factor eEF1B-β has already been discussed in the work describing the NMR structure of human eIF2α in light of the resemblance between eEF1A and aIF2γ (*10*). Since eEF1B-β interacts with eEF1A and fulfills its function by disrupting the magnesium site in the nucleotide binding pocket of the elongation factor (*30*), a possible docking of domain 3 of eIF2α onto the γ subunit was undertaken to discuss the possible participation of this domain in the GDP−GTP exchange reaction in eIF2 (*10*).

Sequence Conservations. To highlight the functionally important regions in e/aIF2α, we searched for residue conservations within all known eukaryotic and archaeal e/aIF2α sequences. The polypeptides were first aligned by using Clustal X (*22*) (Figure 2). In a second step, conservations at each position were analyzed using Plotsimilarity of the GCG package available at the Infobiogen Web site (www.infobiogen.fr). Figure 4 shows that the two best conserved parts are on opposite sides of the protein structure. One area is in domain 1, just within the canonical RNA binding site. The second area is formed by the C-terminal part of β6, the N-terminal part of α9, and the N-terminal part of β8, at the end of domain 3. Domain 2 displays more sequence variability. Only the N-terminal part of helix α6 has a conservation index above the average one.

Biochemical Data. Biochemical experiments in ref *7* showed that domain 3 of aIF2α is responsible for the binding of the α subunit to the γ one. Moreover, the isolated domain 3 proved to be sufficient to confer full Met-tRNA$_i^{Met}$ binding capacity to an αD3γ dimer, as compared to the intact aIF2 trimeric protein. Further, gel shift experiments indicated the capacity of domain 3 to bind either tRNA or rRNA molecules. Therefore, it was proposed that domain 3 reinforces the affinity of aIF2γ for Met-tRNA$_i^{Met}$ through a direct interaction with the polynucleotidic substrate. In gel shift experiments, domain 1 was also shown to possess RNA binding properties. However, in assays measuring the protection against deacylation, this domain appeared not to be involved in the binding of Met-tRNA$_i^{Met}$ (*7*). This domain might therefore be involved in an interaction with either rRNA or mRNA on the ribosome.

Biological Implications. Together, structural homologies, sequence conservations, and biochemical data show that e/aIF2α contains two mobile RNA binding domains playing different roles. The available data suggest that domain 1 of aIF2α interacts with rRNA or mRNA, while domain 3 interacts with the γ subunit and very likely with Met-tRNA$_i^{Met}$. The most conserved part of aIF2α lies in the RNA binding pocket of domain 1. In this context, it is interesting to note that several yeast mutants, having the ability to initiate translation at *HIS4* despite the absence of an AUG start codon, have been selected (*31*, *32*). Mutations affecting eIF2α map to domain 1 (P13S and V19F according to yeast numbering), therefore showing the importance of the β barrel for start codon specificity (*32*). The proline residue is strictly conserved in the e/aIF2α family, and the valine is present in 57 sequences of 66 compared ones. When absent, this valine is replaced with either isoleucine or leucine (eight sequences) or with cysteine in one sequence (Figure 2). In the structure of yeast eIF2α domain 1, the proline and the valine are face to face, in such a way that the mutation of V into F should displace the proline residue. Therefore, even if these residues are not part of the RNA binding site, their mutations are likely to affect the β-barrel conformation and/or stability.

Resolution of the 3D structures of the entire protein from *P. abyssi* and of a derived αD2−3 segment, together with the comparison of these structures with those of human and yeast eIF2α, shows that domain 1 and domain 2 form a rigid body linked to a mobile domain 3. Domain 3 has the capacity to dock the γ subunit of aIF2 (*5*, *7*). Therefore, it can be imagined that upon binding of the aIF2·GTP·Met-tRNA$_i^{Met}$ complex to the ribosome, mobility between domain 3 and domain 1 and 2 bodies helps to inform the e/aIF2γ subunit of contacts between the e/aIF2α subunit and rRNA or mRNA. One piece of information that could be usefully transferred would be the formation of a correct interaction between the CAU anticodon of Met-tRNA$_i^{Met}$ and the AUG start codon presented by mRNA.

ACKNOWLEDGMENT

We thank the staff of the ESRF-JSBG beamlines for assistance during data collection and Thomas Simonson for critical reading of the manuscript.

REFERENCES

1. Hinnebusch, A. G. (2000) in *Translation control of gene expression* (Sonenberg, N., Hershey, J. W. B., and Mathews, M. B., Eds.) pp 185−244, Cold Spring Harbor Laboratory Press, Plainview, NY.
2. Kyrpides, N. C., and Woese, C. R. (1998) Archaeal translation initiation revisited: The initiation factor 2 and eukaryotic initiation factor 2B α-β-δ subunit families, *Proc. Natl. Acad. Sci. U.S.A. 95*, 3726−3730.
3. Schmitt, E., Blanquet, S., and Mechulam, Y. (2002) The large subunit of initiation factor aIF2 is a close structural homologue of elongation factors, *EMBO J. 21*, 1821−1832.
4. Erickson, F. L., Nika, J., Rippel, S., and Hannig, E. M. (2001) Minimum requirements for the function of eukaryotic translation initiation factor 2, *Genetics 158*, 123−132.
5. Roll-Mecak, A., Alone, P., Cao, C., Dever, T. E., and Burley, S. K. (2004) X-ray structure of translation initiation factor eIF2γ: Implications for tRNA and eIF2α binding, *J. Biol. Chem. 279*, 10634−10642.
6. Nissen, P., Kjeldgaard, M., Thirup, S., Polekhina, G., Reshetnikova, L., Clark, B. F. C., and Nyborg, J. (1995) Crystal structure of the ternary complex of Phe-tRNA^{Phe}, EF-Tu, and a GTP analog, *Science 270*, 1464−1472.
7. Yatime, L., Schmitt, E., Blanquet, S., and Mechulam, Y. (2004) Functional molecular mapping of archaeal translation initiation factor 2, *J. Biol. Chem. 279*, 15984−15993.
8. Nonato, M. C., Widom, J., and Clardy, J. (2002) Crystal structure of the N-terminal segment of human eukaryotic translation initiation factor 2α, *J. Biol. Chem. 277*, 17057−17061.
9. Dhaliwal, S., and Hoffman, D. W. (2003) The crystal structure of the N-terminal region of the α subunit of translation initiation factor 2 (eIF2α) from *Saccharomyces cerevisiae* provides a view of the loop containing serine 51, the target of the eIF2α-specific kinases, *J. Mol. Biol. 334*, 187−195.
10. Ito, T., Marintchev, A., and Wagner, G. (2004) Solution structure of human initiation factor eIF2α reveals homology to the elongation factor eEF1B, *Structure 12*, 1693−1704.
11. Perez, J. M., Siegal, G., Kriek, J., Hard, K., Dijk, J., Canters, G. W., and Moller, W. (1999) The solution structure of the guanine nucleotide exchange domain of human elongation factor 1β reveals

a striking resemblance to that of EF-Ts from *Escherichia coli*, *Structure 7*, 217−226.
12. Cousineau, B., Leclerc, F., and Cedergren, R. (1997) On the origin of protein synthesis factors: A gene duplication/fusion model, *J. Mol. Evol. 45*, 661−670.
13. Lindahl, M., Svensson, L. A., Liljas, A., Sedelnikova, S. E., Eliseikina, I. A., Fomenkova, N. P., Nevskaya, N., Nikonov, S. V., Garber, M. B., Muranova, T. A., et al. (1994) Crystal structure of the ribosomal protein S6 from *Thermus thermophilus*, *EMBO J. 13*, 1249−1254.
14. Schenk, P. M., Baumann, S., Mattes, R., and Steinbiss, H. H. (1995) Improved high-level expression system for eukaryotic genes in *Escherichia coli* using T7 RNA polymerase and rare ArgtRNAs, *BioTechniques 19*, 196−200.
15. Leslie, A. (1990) in *Crystallographic computing V*, Oxford University Press, New York.
16. Collaborative Computational Project No. 4 (1994) The CCP4 suite: Programs from protein crystallography, *Acta Crystallogr. D50*, 760−763.
17. Terwilliger, T. C., and Berendzen, J. (1999) Automated MAD and MIR structure solution, *Acta Crystallogr. D55*, 849−861.
18. Terwilliger, T. C. (1999) Reciprocal-space solvent flattening, *Acta Crystallogr. D55*, 1863−1871.
19. Jones, T. A., Zou, J. Y., Cowan, S. W., and Kjeldgaard, M. (1991) Improved methods for the building of proteins model in electron density maps and the location of errors in these models, *Acta Crystallogr. A47*, 110−119.
20. Brunger, A. T., Adams, P. D., Clore, G. M., DeLano, W. L., Gros, P., Grosse-Kunstleve, R. W., Jiang, J. S., Kuszewski, J., Nilges, M., Pannu, N. S., Read, R. J., Rice, L. M., Simonson, T., and Warren, G. L. (1998) Crystallography & NMR system: A new software suite for macromolecular structure determination, *Acta Crystallogr. D54*, 905−921.
21. Storoni, L. C., McCoy, A. J., and Read, R. J. (2004) Likelihood-enhanced fast rotation functions, *Acta Crystallogr. D60*, 432−438.
22. Thompson, J. D., Gibson, T. J., Plewniak, F., Jeanmougin, F., and Higgins, D. G. (1997) The CLUSTAL_X windows interface: Flexible strategies for multiple sequence alignment aided by quality analysis tools, *Nucleic Acids Res. 25*, 4876−4882.
23. Samuel, C. E. (1993) The eIF-2 α protein kinases, regulators of translation in eukaryotes from yeasts to humans, *J. Biol. Chem. 268*, 7603−7606.
24. Nagai, K., Oubridge, C., Jessen, T. H., Li, J., and Evans, P. R. (1990) Crystal structure of the RNA-binding domain of the U1 small nuclear ribonucleoprotein A, *Nature 348*, 515−520.
25. Rosenzweig, A. C., Huffman, D. L., Hou, M. Y., Wernimont, A. K., Pufahl, R. A., and O'Halloran, T. V. (1999) Crystal structure of the Atx1 metallochaperone protein at 1.02 Å resolution, *Structure 7*, 605−617.
26. Jue, R. A., Woodbury, N. W., and Doolittle, R. F. (1980) Sequence homologies among *E. coli* ribosomal proteins: Evidence for evolutionarily related groupings and internal duplications, *J. Mol. Evol. 15*, 129−148.
27. Mosyak, L., Reshetnikova, L., Goldgur, Y., Delarue, M., and Safro, M. G. (1995) Structure of phenylalanyl-tRNA synthetase from *Thermus thermophilus*, *Nat. Struct. Biol. 2*, 537−547.
28. Xiong, Y., and Steitz, T. A. (2004) Mechanism of transfer RNA maturation by CCA-adding enzyme without using an oligonucleotide template, *Nature 430*, 640−645.
29. Jorgensen, R., Ortiz, P. A., Carr-Schmid, A., Nissen, P., Kinzy, T. G., and Andersen, G. R. (2003) Two crystal structures demonstrate large conformational changes in the eukaryotic ribosomal translocase, *Nat. Struct. Biol. 10*, 379−385.
30. Andersen, G. R., Pedersen, L., Valente, L., Chatterjee, I. I., Kinzy, T. G., Kjeldgaard, M., and Nyborg, J. (2000) Structural basis for nucleotide exchange and competition with tRNA in the yeast elongation factor complex eEF1A:eEF1Bα, *Mol. Cell 6*, 1261−1266.
31. Donahue, T. F., Cigan, A. M., Pabich, E. K., and Valavicius, B. C. (1988) Mutations at a Zn(II) finger motif in the yeast eIF-2*β* gene alter ribosomal start-site selection during the scanning process, *Cell 54*, 621−632.
32. Cigan, A. M., Pabich, E. K., Feng, L., and Donahue, T. F. (1989) Yeast translation initiation suppressor sui2 encodes the α subunit of eukaryotic initiation factor 2 and shares sequence identity with the human α subunit, *Proc. Natl. Acad. Sci. U.S.A. 86*, 2784−2788.
33. Fromme, J. C., and Verdine, G. L. (2003) Structure of a trapped endonuclease III-DNA covalent intermediate, *EMBO J. 22*, 3461−3471.
34. Evans, S. V. (1993) Setor: Hardware lighted three-dimensional solid model representation of macromolecules, *J. Mol. Graphics 11*, 134−138.
35. Barton, G. J. (1993) ALSCRIPT: A tool to format multiple sequence alignments, *Protein Eng. 6*, 37−40.
36. Nicholls, A., and Honig, B. (1991) A rapid finite difference algorithm utilizing successive over-relaxation to solve the Poisson−Boltzmann equation, *J. Comput. Chem. 12*, 435−445.
37. Nicholls, A., Sharp, K. A., and Honig, B. (1991) Protein folding and association: Insights from the interfacial and thermodynamic properties of hydrocarbons, *Proteins 11*, 281−286.
38. Koradi, R., Billeter, M., and Wuthrich, K. (1996) MOLMOL: A program for display and analysis of macromolecular structures, *J. Mol. Graphics 14*, 51−55.

BI050373I